Published in final edited form as:
Structure. 2012 April 4; 20(4): 604–617. doi:10.1016/j.str.2012.02.001.

Solution structure analysis of the HPV16 E6 oncoprotein reveals a self-association mechanism required for E6-mediated degradation of p53

Katia Zanier[(1),(&)], **Abdellahi ould M'hamed ould Sidi**[(1)], **Charlotte Boulade-Ladame**[(1)], **Vladimir Rybin**[(2)], **Anne Chappelle**[(1)], **Andrew Atkinson**[(3)], **Bruno Kieffer**[(3),1], and **Gilles Travé**[(1),1,(&)]

[(1)]Institut de Recherche de l'Ecole de Biotechnologie de Strasbourg (IREBS), Boulevard Sébastien Brant, BP 10413, 67412 Illkirch, France

[(2)]European Molecular Biology Laboratories (EMBL), Heidelberg, Meyerhofstrasse 1, 69117 Heidelberg, Germany

[(3)]Institut de Génétique et de Biologie Moléculaire et Cellulaire (IGBMC), 1 rue Laurent Fries, BP 163, 67404 Illkirch, France

Abstract

The viral oncoprotein E6 is an essential factor for cervical cancers induced by "high-risk" mucosal HPV. Among other oncogenic activities, E6 recruits the ubiquitin ligase E6AP to promote the ubiquitination and subsequent proteasomal degradation of p53. E6 is prone to self-association, which long precluded its structural analysis. Here we found that E6 specifically dimerizes through its N-terminal domain and that disruption of the dimer interface strongly increases E6 solubility. This allowed us to raise the first structural data covering the entire HPV16 E6 protein, including the high-resolution NMR structures of the two zinc-binding domains of E6 and a robust data-driven model structure of the N-terminal domain homodimer. Interestingly, homodimer interface mutations that disrupt E6 self-association also inactivate E6-mediated p53 degradation. These data suggest that E6 needs to self-associate via its N-terminal domain to promote the poly-ubiquitination of p53 by E6AP.

Keywords

cervical cancer; E6; HPV; oncoprotein; p53 degradation; self-association

INTRODUCTION

Human Papillomaviruses (HPV) are small DNA viruses that induce squamous epithelial neoplasia. Over 120 HPV types have been identified featuring distinct tropisms for different body sites (skin, mouth and genitalia) (de Villiers et al., 2004). HPVs can be divided into

[(&)]Corresponding authors: Phone: +33 3 68 85 44 06, fax: +33 3 68 85 47 18 zanier@unistra.fr, trave@unistra.fr.

[1]B.K. and G.T. equally contributed to the supervision of this work.

The authors declare they have no conflict of interests.

"low-risk" and "high-risk" types according to the propensity of the lesions to evolve into malignancies. 'High-risk' mucosal HPVs are the causative agents of cervical cancers, with HPV16 and HPV18 being the most common oncogenic types associated with 50% and 20% of the carcinomas respectively (Bosch et al., 1995). In HPV-positive cervical carcinomas, two viral genes, E6 and E7, are expressed and act cooperatively to promote tumorogenesis. The HPV E6 oncoprotein interacts with several cellular proteins, thereby activating a number of oncogenic pathways that lead to blockage of apoptosis, alterations of the transcription machinery, interference with cell-cell interactions and cell immortalization (Chakrabarti and Krishna, 2003). One of the most investigated oncogenic activities of "high-risk" mucosal HPV E6 proteins is the ability to inactivate the tumor suppressor p53 by targeting it to degradation (Werness et al., 1990). E6 has been found to recruit the E3 ubiquitin ligase E6AP (Huibregtse et al., 1991; Scheffner et al., 1993) by binding to a conserved LXXLL motif located in a presumably natively unfolded region of the ligase (Chen et al., 1998; Huibregtse et al., 1993). This binding event alters E6AP substrate specificity *via* an unknown mechanism that allows recruitment and polyubiquitination of p53, which is subsequently degraded by the 26S proteasome (Scheffner et al., 1995). In addition to p53, other host cell proteins are recruited and sometimes targeted for ubiquitin-mediated degradation by "high-risk" mucosal HPV E6. Among these targets are proteins containing multiple PDZ domains that bind to the C-terminus of E6, which include the tumour suppressor human discs large (hDlg) (Kiyono et al., 1997) and the MAGI family of proteins (Glaunsinger et al., 2000; Thomas et al., 2002), the pro-apoptotic protein Bak (Thomas and Banks, 1998) and c-Myc (Gross-Mesilaty et al., 1998). Recent studies suggest that additional E6 mediated p53 degradation pathways might exist that are independent of E6AP ligase activity (Camus et al., 2007; Massimi et al., 2008; Nomine et al., 2006; Shai et al., 2007). In addition, putative mechanisms modulating E6-mediated degradation have been proposed, which include proteasome-mediated degradation of both E6 (Stewart et al., 2004) and E6AP (Kao et al., 2000), stabilization of E6 by E6AP (Tomaic et al., 2009), E6 interaction with the deubiquitinating enzyme USP15 (Vos et al., 2009) and inhibition of the E6/E6AP activity by the EDD ubiquitin ligase (Tomaic et al., 2011).

HPV E6 proteins are rather small in size (about 150 amino acids) and share a common architecture consisting of two zinc-binding domains (E6N and E6C) (Nominé et al., 2003). For HPV16 the E6N domain undergoes homodimerization (Lipari et al., 2001), whereas the E6C domain remains monomeric at high concentrations (Nominé et al., 2005). We and others have observed that E6 proteins from different phylogenetic viral groups undergo self-association *in vitro* (Garcia-Alai et al., 2007; Nominé et al., 2001b; Zanier et al., 2007), generating oligomeric species with native-like properties with respect to domain folds and activities (Zanier et al., 2010) and *in vivo* upon transfection in eukaryotic cells (Garcia-Alai et al., 2007; Zanier et al., 2010). This latter property of E6 proteins has for a long time precluded structural work on this oncoprotein. Consequently, to date the structural data available on E6 proteins is limited to one single NMR structure, describing the E6C domain of HPV16 (Nomine et al., 2006).

In this work we raised for the first time high-resolution structural data covering the entire HPV16 E6 protein by solving the NMR structure of the E6N domain, calculating a data-driven model of the E6N homodimer and revisiting the NMR structure of the E6C domain. Site-directed mutagenesis at the E6N homodimer interface revealed by the structures strongly suggests that E6 self-association mediated by the E6N region is necessary in the process of p53 degradation.

RESULTS

Characterization of the E6N homodimer

The HPV16 E6N domain (residues 1-80) was expressed and purified according to the protocols developed for E6 proteins (Zanier et al., 2007). $^{1}H,^{15}N$-HSQC NMR spectra were acquired on the E6N domain at concentrations ranging between 300 μM, which is the maximal concentration attained by this construct, and 25 μM. Spectra comparison shows that amide groups belonging to residues H24, E41, Y43, D44 and F47 experience significant chemical shift displacements upon dilution (>60 Hz) (Figure 1A). In parallel, analytical ultracentrifugation velocity experiments reveals the existence of monomeric and dimeric species in samples of the E6N domain (Figure 1B, black line). By contrast, a mutated E6N domain bearing the F47R substitution turns out to be monomeric in ultracentrifugation experiments (Figure 1B, red line). We thus fitted the chemical shift perturbation data of the wild-type domain to the standard equation for monomer-dimer equilibrium, yielding an equilibrium dissociation constant (K_D) of 290 ± 120 μM (Figure 1C). Comparable monomer-dimer affinity values have been obtained from equilibrium ultracentrifugation experiments for a similar construct of HPV16 E6N (Lipari et al., 2001).

Next, we applied standard triple resonance NMR methods to fully assign backbone and side-chain resonances of wild-type E6N both at 150 μM and 300 μM concentrations, as well as those of the monomeric E6N F47R construct. The similarities of the $^{1}H,^{15}N$-HSQC spectra and of the secondary carbon chemical shift values of wild-type and E6N F47R indicate that the two constructs have very similar structures (Figure S1 A and B). The differences in composite ^{1}H, ^{13}C and ^{15}N chemical shifts were then computed, either between diluted and concentrated wt E6N or between concentrated wt E6N and E6N F47R (Figure 1D). The resulting profiles are remarkably similar, showing that the mutation destabilizes dimerization similarly to dilution, without altering the conformation of the domain. This allowed us to precisely identify the residues at the dimer interface: I23, H24, R39, R40, E41, Y43, D44, A46 and F47.

NMR structures of E6N and E6C domains

Line-broadening phenomena likely resulting from transient dimerization of the HPV16 E6N domain significantly affect the quality of the NMR spectra. By contrast, the monomeric E6N F47R mutant is an optimal target for structure determination, displaying improved line-widths (Figure S1C). We therefore proceeded to determine the solution structure of the monomeric E6N F47R mutant domain. In addition, we applied triple resonance NMR to revisit the structure of the monomeric HPV16 E6C 4C/4S mutant domain (residues 80-151), which had been previously solved using only homonuclear and double resonance NMR (Nomine et al., 2006). Thanks to the ^{13}C-editing we were now able to correct the assignments of a small number of side-chain resonances of the E6C 4C/4S construct.

The resulting structures are well-defined with an average of 15 and 19 noe restraints per residues for the E6N and E6C domains respectively (Table 1). The pairwise r.m.s. deviation for backbone atoms of residues 12 to 71 of the E6N domain is 0.82 Å, while residues 72-80, comprising the interdomain linker, are unstructured (Figure 2A). Similarly the E6C domain has residues 80 to 143 well-defined with a backbone r.m.s. deviation of 0.56 Å and the C-terminal residues 144-151 unstructured (Figure 2B). Noteworthily, the structures reveal that the F47R substitution and the four cysteine-serine mutations are all directed at solvent exposed residues (see Figure 3B), further reinforcing the view that these mutations do not alter the conformation of the domains.

The overall fold of the E6C domain remains as previously described except a few modifications in the positioning of secondary structure elements (Figure S2). These

modifications do not alter the surface properties of the domain, which were the main feature put forward in our former analysis of this construct (Nomine et al., 2006) (see below for further discussion).

The E6N fold consists of a three-stranded β-sheet and three α helices. The zinc-binding site is peripheral with two liganded cysteines contributed by a knuckle, which provides one strand (β 1) to the β-sheet, and the other two situated in the C-terminal helix. The N-terminal region, corresponding to residues 1 to 10, adopts an extended and rather flexible structure as indicated by the low ^{1}H-^{15}N heteronuclear NOE values, which correlate with dynamic events in the nanosecond timescale. Such dynamic properties are reflected in the poorer definition in the NMR ensemble, as shown by the larger backbone r.m.s. deviations (Figure 3A). However, in spite of the backbone flexibility, we could observe long-range NOE contacts between the aromatic protons of F2 and the side-chains of core residues P9, L15, L19, Y54 and P59. These constraints place the aromatic ring of F2 in a well-defined position, anchoring the flexible N-terminal region to the hydrophobic core (Figure 3A).

The structures of the HPV16 E6N and E6C domains are homologous with the exception of the N-terminal regions (Figure 3B). Whereas the N-terminal region of E6N is a flexible loop, the N-terminus of E6C (residues 80-84) folds into an additional β-strand (β0), which extends the β-sheet. In spite of the structural homology, the surface properties of the two domains differ (Figure S3). While the E6N domain has both acidic and basic regions, the E6C domain is mostly positively charged. Concerning surface hydrophobicity, we observe two distinct hydrophobic regions at opposing sides of E6N, one corresponding to residues located on the β-2 strand, the zinc-binding hairpin and helix 3, the other one mostly consisting of the E6N homodimerization surface discussed below (Figure S3A). For E6C, exposed hydrophobic residues cluster within a unique region as previously described by Nominé *et al.* (compare Figure S3B and Figure 1 in (Nomine et al., 2006)).

NMR data driven model of the E6N homodimer

We proceeded to investigate the assembly of the HPV16 E6N homodimer using the HADDOCK software (Dominguez et al., 2003). Ambiguous interaction restraints (AIRs) defined from chemical shift perturbation data were used to calculate a first set of E6N homodimer models. Subsequently, we analyzed wild-type E6N NOESY spectra acquired at different concentrations. This allowed us to identify 11 unambiguous intermolecular NOEs that were consistent with the best scoring cluster of homodimer models. All intermolecular NOEs originate from contacts of the aromatic protons of F47 with protons from residues I23, H24 and Y43 (Figure S4A). Hence, intermolecular NOE-derived distance restraints were combined with AIRs to calculate a final set of E6N homodimer model structures that were grouped into three clusters, all fulfilling equally well the NMR data and displaying similar subunit arrangements (Figure S4 B and C). The top-scoring cluster (cluster 1) contains the 65% of the structures. Statistics for the 20 best models in cluster 1 are reported in Table 2.

The homodimer interface corresponds to helix α2 and the loop region between helix1 and the zinc knuckle. In all models calculated F47 appears to dominate the homodimer interface, with its aromatic ring lying in a shallow hydrophobic cavity made of residues I23, H24, Y43, A46 and F47 of the opposing subunit (Figure 4A). In some of the structures the side-chains of arginine and aspartic acid residues at the homodimer interface engage in both intra-(R48/D44) and inter-molecular (R39/D64) ionic bridges (Figure 4A). Although poorly defined in the structure ensemble due to the lack of NOEs, these ionic interactions are consistent with the observation of a larger extent of protection of arginine side-chain exchangeable protons in the NMR spectra of the wt E6N homodimer compared to the E6N F47R monomer (Figure S4D).

Alignment of E6N sequences from different phylogenetic PV groups shows that the hydrophobic/aromatic character of residues I23, Y43 and F47 participating in key intermolecular interactions is conserved in both 'high-risk' and 'low-risk' mucosal HPV strains from the A9, A7 and A10 species, while most charged and polar residues (R39, R40, D44 and D64) of the interface are less conserved, with the exception of E41 that is strictly conserved in all papillomaviruses, probably due to its structural role (helix capping for α3) (Figure 4B). To further investigate conservation of E6N dimerization, we analyzed samples of E6N domains issued from different groups. The isolated E6N domains from HPV18, HPV5 and BPV1 strains could be purified at high concentrations and were folded according to the chemical shift dispersion observed in the $^{1}H,^{15}N$-HSQC spectra (*data not shown*). According to the analytical ultracentrifugation profiles (Figure 4C, left panel), while the HPV18 E6N domain (residues 1-82) undergoes dimerization, both the HPV5 (residues 1-91) and BPV1 E6N domains (residues 1-66) are clearly monomeric. The HPV11 E6N domain (residues 1-81) was poorly soluble in isolation. To turn around this problem we analyzed this domain as a fusion to the MBP tag, which allowed it to attain higher concentrations. Analytical gel filtration chromatography of the HPV11 MBP-E6N construct shows a progressive shift from a monomeric to a dimeric species with increasing sample concentration (Figure 4C, right panel). This latter analysis suggests an equilibrium affinity of dimerization in the same range as that of the HPV16 E6N dimer. Therefore these results support the view that E6N homodimerization is a property of E6 proteins from both 'high-risk' and 'low-risk' mucosal HPV strains.

Disruption of E6N dimerization decreases self-association of full-length E6

We were interested in probing the role of the E6N dimerization region with respect to the self-association of full-length E6. For this purpose, we generated a panel of E6N constructs that, like E6N F47R, bear single point mutations at the dimer interface (H24A, Y43R, Y43E, D44A, D44R, and F47E). All constructs were folded according to the $^{1}H,^{15}N$-HSQC spectra (*data not shown*). E6N mutants were then submitted to analytical ultracentrifugation velocity experiments (Figure 5A). As expected, all mutations turn out to weaken dimerization. Substitutions of Y43 and F47 with both arginine and glutamic acid disrupt dimerization, in agreement with the hydrophobic role of these residues revealed by the dimer structures. However, the peaks of the F47E and Y43E mutants are shifted towards higher molecular weight compared to those of the arginine substitutions, reflecting the existence of residual monomer-dimer equilibrium and therefore a lower efficiency of glutamic acid in disrupting dimerization. Similarly the D44R mutation destabilizes the dimeric state more efficiently than D44A. These latter observations indicate the existence of ionic interactions at the dimer interface, which is also suggested by the structural data.

Next we introduced E6N dimer destabilizing mutations in the context of a mutant of HPV16 E6, named E6 4C/4S, which bears the same four cysteine-serine substitutions as the E6C domain used for structure determination. Whereas wild-type HPV16 E6 cannot be purified due to extensive intermolecular disulfide cross-linking (Nominé et al., 2001a), E6 4C/4S is amenable to purification. Moreover, E6 4C/4S retains a p53 degradation activity profile very similar to that of HPV16 wt E6 (Figure S5A). The concentration thresholds of E6 4C/4S constructs bearing E6N dimer destabilizing mutations were then determined by concentrating purified samples of the constructs to their solubility limit (Figure 5B). All E6N dimer mutations were found to enhance the solubility of E6 4C/4S, although to a different extent. While only a moderate enhancement is observed for the Y43R and D44R mutations, F47 mutations greatly increase E6 solubility, with the arginine being more efficient than glutamic acid as already observed for E6N dimerization. Further solubilization of E6 is obtained with the double F47R-Y43E mutation.

NMR characterization of monomeric full-length E6

The enhanced solubility of E6 F47R 4C/4S allowed us to perform the first NMR analysis of a full-length HPV E6 protein. Superimposition of the $^{1}H,^{15}N$-HSQC spectrum of E6 F47R 4C/4S onto those of the E6N F47R and E6C 4C/4S domains shows that most amide signals of the full-length E6 construct overlay with signals in its separated domains (Figure 5C, left panel), indicating that the structures of the domains are preserved in the context of the full-length protein. By combining this information with triple resonance backbone experiments, we could assign approximately 92% of the backbone frequencies of the full-length E6 F47R 4C/4S construct (Figure 5C, right panel). Most missing resonances correspond to the interdomain linker, which experiences line broadening likely to result from dynamic processes. T1 and T2 NMR relaxation experiments were then recorded on a maximally concentrated sample of E6 F47R 4C/4S (Figure S5B). This raised a tumbling correlation time (τc) of 13 ± 1.5 ns at 296 K, which is consistent with a 18 kDa protein tumbling as a rigid monomer. Noteworthily, independent tumbling of E6N and E6C domains would lead to a correlation time of 6-8 ns, consistent with the value measured previously for the E6C 4C/4S domain (7.8 ± 1.5 ns at 285 K) (Nominé et al., 2005).

Correlation of E6 self-association and p53 degradation activities

We have previously reported that the F47R mutation leads to loss of the p53 degradation activity of HPV16 E6 (Nomine et al., 2006; Ristriani et al., 2009). Here we have extended the analysis to the other E6N dimerization mutants inserted in the E6 4C/4S construct and already presented in Figure 5. Consistent with what has been previously reported for the F47R mutation, all mutants have wild-type like binding activities to both E6AP-peptide and full-length E6AP in GST pull-down assays, suggesting that the E6N dimerization interface is not implicated in the recruitment of the ubiquitin ligase (Figure S6A). We then performed a quantitative analysis of the *in vitro* p53 degradation activities of the different mutants by incubating constant amounts of translated and ^{35}S-labelled p53 with varying amounts of ^{35}S-labelled E6 translation products. In such assays, E6-mediated p53 degradation activity is measured by the loss of intensity of p53 bands. The most active E6 constructs are those, which can degrade p53 at the lowest E6 amounts. While both wild-type E6 and E6 4C/4S have comparable activity profiles (with the 4C/4S construct slightly more active, maybe due to protection from disulfide cross-linking), all mutations at the E6N homodimer interface affect p53 degradation albeit at different extents (Figure 6A and Figure S6B). While D44R and Y43R mutations have lower impact, mutations at F47 largely suppress p53 degradation activity. We also performed an *in vivo* assay that makes use of co-transfection in human C33A cells followed by double immunofluorescence with anti-E6 and anti-p53 antibodies (Figure 6B). The disappearance of the *red* p53 signal in the *green* E6-transfected cells indicates E6-mediated p53 degradation. In this assay, the *in vivo* p53 degradation activities of the different mutants are ranked similarly as the *in vitro* activities.

Next, we plotted p53 degradation activities as a function of solubility thresholds for all E6 mutants. Interestingly, we find a remarkable correlation between these two observables: the higher the concentration threshold value, the lower the p53 degradation activity (Figure 6C). These observations suggest that formation of a dimeric or oligomeric species of E6 may be required for p53 degradation.

DISCUSSION

E6, one of the most studied oncoproteins, has long represented a challenge for structural biologists. In this work we adopted a “divide, mutate and conquer” approach whereby we not only separated the two folded domains of E6, but also mutated them to suppress their self-association properties. This allowed us to solve high-resolution structures of both E6N

and E6C domains, to raise a robust data-driven model of the E6N homodimer, and to obtain the first structural information on full-length E6.

The low solubility of E6 proteins was a multifactorial problem. First, E6 proteins are rich in cysteine residues prone to form intermolecular disulfide bridges during purification. This initially drove us to mutate all non-conserved cysteines, generating the HPV16 E6 6C/6S construct (Nominé et al., 2001a) as well as comparable mutants for other E6 proteins (Zanier et al., 2007). E6 6C/6S retains the capacity to degrade p53 albeit with lower efficiency than HPV16 wt E6, whereas E6 4C/4S fully retains the efficiency of E6 wt (Supplementary Figure 8). This finding is explained by the structure: the four mutated cysteine residues in E6C 4C/4S are solvent-exposed, whereas the two non-conserved cysteine residues of E6N are buried and hence prone to destabilize E6 when mutated (Figure 2B). Second, as previously suggested by Liu et al. (Liu et al., 2009), the E6N domain plays a role in E6 aggregation. Here we characterized the E6N dimer and showed that its disruption greatly enhances E6 solubility, pointing to E6N dimerization as a key event for E6 oligomerization/polymerization. Third, E6 probably captures its target “LxxLL” motifs by means of a hydrophobic pocket, which may promote aggregation of unbound E6. Indeed, we recently showed that aggregation of Bovine (BPV1) E6 is eliminated when BPV1 E6 is bound to its target LxxLL peptide (Ould M’hamed Ould Sidi et al., 2011). Noteworthily, cysteine mutagenesis did not solubilize BPV-1 E6, and BPV1 E6N does not dimerize, suggesting that BPV-1 E6 aggregation is mainly driven by its LxxLL-binding pocket. Conversely, binding of HPV16 E6 to a peptide containing the LXXLL motif from E6AP did not enhance HPV16 E6 solubility. Therefore, E6 self-association phenomena are not only due to multiple causes, but also require distinct remedial strategies depending on the E6 protein considered.

The two zinc-binding domains of HPV16 E6 have homologous folds. Both domains contain a derived version of the treble cleft motif found in a large number of zinc-binding proteins with diverse functions (de Souza et al., 2010; Grishin, 2001). However, the ten first residues of E6N adopt an extended and flexible conformation that is “anchored” to the rest of the domain structure by the aromatic ring of F2, whereas the corresponding region in E6C folds into an additional β-strand. Early work in our laboratory showed that antibodies targeting residue F2 of HPV16 E6 block degradation of p53 (Giovane et al., 1999), while other studies demonstrated that point mutations at residue F2 abolish recruitment of p53 to the HPV16 E6/E6AP complex and hence the degradation of p53 (Cooper et al., 2003; Liu et al., 1999). Thus, the flexible N-terminal region of E6N, and particularly the anchoring residue F2, appears to be implicated in p53 degradation mediated by “high-risk” mucosal HPV E6 proteins. Interestingly, the N-terminal region of E6N is the least conserved part of PV E6 proteins, both in composition and in length (Figure 4B), suggesting that it may have specialized to allow targeting of distinct sets of cellular proteins.

Within full-length monomeric E6, the structures of E6N and E6C domains are preserved and their tumbling is correlated. How and to which extent both domains interact with each other in the full-length protein is not yet known. Unfortunately, spectra of monomeric E6 remained significantly affected by line-broadening, preventing the completion of the entire 3D structure. We previously proposed (Nomine et al., 2006) a “pseudodimeric” model of E6, which assumed that E6N and E6C domains would associate symmetrically *via* their respective N-terminal β-strands (β0 in E6C). However, the structure of E6N does not contain a N-terminal β-strand. In addition, the chemical shifts of most amide groups in the N-terminal regions of both domains (indicated by arrows in Figure 5C) are not displaced in the spectrum of the full-length E6 construct. This suggests that the N-termini of both domains neither change conformation nor interact with each other in the full-length protein, therefore contradicting the pseudodimeric model previously proposed.

The E6N homodimer structure together with the mutational data reveals that key interface interactions are mediated by F47 that lays in a hydrophobic cavity mainly formed by surface residues I23, Y43 and F47 of the opposing subunit. The hydrophobic/aromatic character of these three residues is conserved only in mucosal HPV E6 sequences (Figure 4B), suggesting that E6N dimerization is an activity specific to the mucosal HPV strains rather than a general property of all E6 proteins. Indeed, E6N domains of “high-risk” mucosal HPVs 16 and 18 (belonging to two distinct species) and of ‘low-risk’ mucosal HPV11 were found to dimerize, whereas the E6N domains of the cutaneous strains HPV5 and BPV1 (a bovine PV) were found to be monomeric.

In the last part of this work we have investigated the importance of E6N homodimerization for E6 activities leading to p53 degradation. Interface mutations disrupted E6N dimerization and enhanced full-length E6 solubility by favouring its monomeric state as demonstrated for the E6 F47R 4C/4S construct. Interface mutants displayed unaltered E6AP binding but were found to be defective for p53 degradation activity. A striking correlation was observed between the solubility thresholds and the p53 degradation activities for all full-length E6 mutants investigated. This suggests that a dimeric E6 is required to efficiently catalyze the degradation of p53. Indeed, we have previously reported on the F47R mutation at times when E6N dimerization had not been investigated (Nomine et al., 2006; Ristriani et al., 2009; Zanier et al., 2005). Although able to recruit p53 to the E6/E6AP complex, E6 F47R was defective for poly-ubiquitination and subsequent degradation of p53 (Ristriani et al., 2009). On the basis of the results presented in this work, together with our previous findings on the F47R mutant, we therefore propose that the enzyme (E6AP) and the substrate (p53) are recruited onto a symmetric dimer of E6 (Figure 6). In this model the relative orientations of the p53 and E6AP subunits are different when bound to the same or different E6 molecules. Only E6AP and p53 bound to different E6 molecules would then associate in a way that is sterically compatible with the trans-ubiquitination event leading to degradation of p53. An interesting implication of this dimeric model is that its inherent symmetry would allow for allosteric regulation possibly resulting in enhanced enzymatic efficiency. This model is in agreement with our observation that heterologously expressed E6 self-associates *in vivo* (Zanier et al., 2010), and it is also supported by data from Kao *et al.* (Kao et al., 2000), who detected intermolecular interactions between E6AP molecules mediated by E6. Further investigation will be required to precisely address the *in vivo* role of E6 dimerization.

We have found that ‘low-risk’ mucosal HPV11 E6, which is unable to degrade p53, also dimerizes *via* its E6N domain. Hence E6N dimerization appears to be a necessary but not sufficient condition to achieve E6-mediated p53 degradation. Remarkably, HPV11 E6 has also been reported to bind to E6AP (Brimer et al., 2007) and to p53 (Gu et al., 2001; Li and Coffino, 1996; Thomas and Chiang, 2005). However, these authors also suggested that the interfaces between E6, p53 and E6AP are probably involving different regions for HPV16 and HPV11 E6 proteins, in a manner that p53 ubiquitination is only proficient for the HPV16 E6-mediated complexes.

By contrast, it seems that dimerization is not required for the degradation of all targets of E6. For instance, protein tyrosine phosphatase H1 (PTP H1) is degraded by E6 *via* a mechanism requiring E6AP and the proteasome machinery (Jing et al., 2007; Topffer et al., 2007) and this process is unaffected by the F47R mutation.

The results presented in this work contribute to the understanding of the assembly and mechanisms of E6 ubiquitination proficient complexes. The fact that the E6 dimerization interface is required for p53 degradation, but not for all targets of the E6/E6AP complex,

suggests that a proficient E6/E6AP/p53 complex requires a particular assembly mechanism that will deserve to be addressed in future structural studies.

MATERIALS AND METHODS

Preparation of recombinant HPV E6 samples

The DNA sequences of E6 constructs for recombinant production were cloned in the NcoI and KpnI sites of the pETM-41 vector containing an N-terminal His_6-MBP tag followed by a TEV cleavage site.

Over-expression of full-length E6 and E6 domain constructs fused to MBP was carried out overnight in BL21 DE3 cells at 15 °C. Uniform $^{13}C/^{15}N$ isotope labelling was achieved by supplementing minimal M9 medium (containing $^{15}NH_4Cl$ and $^{13}C_6$-glucose) with 5% CELTONE-CN medium (CIL Inc.). The purification protocol described in (Zanier et al., 2007) was supplemented with a final gel filtration chromatography step on a Superdex75 10/60 column (GE Healthcare).

Analytical ultracentrifugation

Sedimentation velocity experiments were done at 4 °C in a Beckman Optima XL-A centrifuge fitted with a four-hole AN-60 rotor and double-sector Epon centrepieces (46 000 rpm**)**. Protein concentrations were adjusted to 70 μM in 20 mM sodium phosphate (pH 6.8), 50 mM NaCl, 2 mM DTT. Sedimentation velocity profiles were collected by monitoring the absorbance signal at 280 nm. Sedimentation coefficient and molecular weight distributions were analysed by the C(s) method implemented in the Sedfit software package (Schuck, 2000).

Analytical gel filtration chromatography

HPV11 MBP-E6N preparations were affinity purified and subject to an overnight ultracentrifugation step as described in (Zanier et al., 2007). Sample concentrations were adjusted to values ranging from 40 to 800 μM. 100 μl aliquots were injected on a Superdex 200 10/30 column (GE Healthcare) equilibrated in 20 mM sodium phosphate (pH 6.8), 400 mM NaCl, 2 mM DTT. The higher salt concentration was employed to avoid aspecific interaction of MBP-E6N with the column matrix. The experiments were performed at 10 °C.

NMR spectroscopy

NMR experiments were recorded on a Bruker DRX 600 MHz spectrometer equipped with cryoprobe (unless otherwise stated) at 296 K for the wt and E6N F47R domains and for the full-length E6 F47R 4C/4S construct and at 283 K for the E6C 4C/4S domain. Buffer composition for the E6N and E6C domain NMR samples was 20 mM sodium phosphate (pH 6.8), 50 mM NaCl, 2 mM DTT. For the full-length E6 samples the NMR buffer was 20 mM sodium phosphate (pH 6.8), 200 mM NaCl, 2 mM DTT. Backbone and side-chain assignments of wt E6N, E6N F47R and E6C 4C/4S constructs were derived using triple resonance NMR methods (Sattler et al., 1999). Heteronuclear ^{1}H-^{15}N NOE values for the E6N F47R construct were derived from intensities measured using the experiment described by *Farrow et al.* (Farrow et al., 1994).

Structure calculations of E6 domains

Structure calculations for the E6N F47R and E6C 4C/4S domains were performed using XPLOR-NIH (Schwieters et al., 2003) and ATNOS/CANDID for automatic peak picking and NOE assignment (Herrmann et al., 2002a; Herrmann et al., 2002b). Distance restrains were derived from 2D homonuclear NOESY spectra with mixing times of 100 ms recorded

at 800 (E6N F47R) and 950 (E6C 4C/4S domain) MHz and from 3D ^{15}N-edited and ^{15}C-edited NOESY spectra (optimized for aliphatic nuclei) with mixing times of 100 ms. Dihedral angle restraints for φ and ψ angles were derived from Cα and Cβ chemical shifts using the program TALOS (Cornilescu et al., 1999). Hydrogen bond restrains were derived from slowly exchanging amide protons upon dilution of concentrated samples into D_2O buffer. Zn-Sγ distances were set to 2.4 Å. The structures were then refined using parallhdg5.3 parameters (Linge et al., 2003; Nabuurs et al., 2004) and chirality assignments were made before water refinement. The final ensembles of 20 conformations for the E6N F47R and E6C 4C/4S domains have no NOE violations greater than 0.5 Å and no dihedral angle violations greater than 5°. Ramachandran plot analysis was performed using PROCHECK (Laskowski et al., 1996).

Calculation of the E6N homodimer

Structure calculations for the E6N homodimer were performed using the HADDOCK webserver (de Vries et al., 2010; Dominguez et al., 2003). Starting coordinates were the 10 lowest energy NMR structures of E6N F47R, with each structure in the ensemble back mutated *in silico* to produce the wild-type domain. Ambigous interactions restraints (AIRs) were derived from the changes in the chemical shifts of assigned ^{1}H, ^{13}C and ^{15}N resonances.

The approach adopted used initial modelling to guide identification of intermolecular NOEs. In a first set of calculations only AIRs were used during the docking steps. The resulting models were hierarchically clustered into 5 distinct clusters. Weak intermolecular NOEs were identified from 2D homonuclear NOESY spectra recorded on samples at 300 to 150 μM of wt E6N at 700 MHz with mixing times of 100, 150 and 200ms. The identified intermolecular NOEs satisfied the following conditions: (i) they decreased in intensity upon dilution of the sample, (ii) they were consistent with E6N homodimer models in the top scoring cluster of the HADDOCK calculations and, finally, (iii) they originated from proton pairs separated by more than 8 Å in the monomer structure. In the final calculations AIRs, unambigous intermolecular NOE-derived restraints (applied with generous error bounds, i.e. 3.9 ± 2.1 Å) as well as dihedral angle restraints were enforced during all docking steps. During the first iteration, 1000 models were calculated keeping the domain structure rigid. The 200 lowest energy models were then submitted to semi-flexible torsion angle simulated annealing in the second iteration and finally refined in explicit solvent. The final structures were clustered using a cut-off value of 5 Å and a minimum cluster size of 10 structures. The 20 lowest energy structures from the HADDOCK top-scoring cluster (cluster 1) have no NOE violations greater than 0.1 Å and no dihedral angle violations greater than 5°.

p53 degradation assays

HPV16 E6 mutants were cloned in the BamHI and KpnI sites of the pXJ40 vector. *In vitro* p53 degradation reactions were performed by incubating 2 μl of ^{35}S p53 translation product with varying amounts (5-0.37 μl) of ^{35}S E6 translation products at 28 °C for 2 hours according to previously described protocols (Nomine et al., 2006). Reactions were analyzed by SDS-PAGE and autoradiography. Bands were quantified using a Gel Doc (1000 UV)XR + apparatus (Biorad). *In vivo* p53 degradation assays were performed by transfecting human C33A cells with HPV16 E6 mutants as described in (Nomine et al., 2006). Simultaneous observation of p53 and E6 was achieved by incubating cells first with polyclonal anti-p53 antibody (FL393, Santa Cruz Biotechnology) and then with monoclonal anti-E6 antibody 6F4 (Masson et al., 2003).

Data deposition

Atomic coordinates for the structures have been submitted to the PDB/BMRB databases and assigned the identifiers 2ljx (E6N), 2ljz (E6C) and 2ljy (E6N dimer).

Supplementary Material

Refer to Web version on PubMed Central for supplementary material.

Acknowledgments

We are grateful to S. Vande Pol and A. Mc Ewen for useful comments and suggestions. We thank G. Stier for providing vectors. A. ould M'hamed ould Sidi was supported by a fellowships from ARC. This work was funded by the following organizations: Centre National de la Recherche Scientifique (CNRS), Association pour la Recherche sur le Cancer (grant ARC-2007 3171) National Institute of Health (grant NIH R01CA134737), Ligue Nationale Contre le Cancer, Agence Nationale de la Recherche (ANR-06-BLAN-0404 and ANR-MIME-2007 EPI-HPV-3D), Fondation pour la Recherche Médicale (FRM) and Arbor Vita Corporation (Sunnyvale, CA).

REFERENCES

Bosch FX, Manos MM, Munoz N, Sherman M, Jansen AM, Peto J, Schiffman MH, Moreno V, Kurman R, Shah KV, International biological study on cervical cancer (IBSCC) Study Group. Prevalence of human papillomavirus in cervical cancer: a worldwide perspective. J. Natl. Cancer Inst. 1995; 87:796–802. [PubMed: 7791229]

Brimer N, Lyons C, Vande Pol SB. Association of E6AP (UBE3A) with human papillomavirus type 11 E6 protein. Virology. 2007; 358:303–310. [PubMed: 17023019]

Camus S, Menendez S, Cheok CF, Stevenson LF, Lain S, Lane DP. Ubiquitin-independent degradation of p53 mediated by high-risk human papillomavirus protein E6. Oncogene. 2007; 26:4059–4070. [PubMed: 17224909]

Chakrabarti O, Krishna S. Molecular interactions of 'high-risk' human papillomaviruses E6 and E7 oncoproteins: implications for tumour progression. J. Biosci. 2003; 28:337–348. [PubMed: 12734411]

Chen JJ, Hong Y, Rustamzadeh E, Baleja JD, Androphy EJ. Identification of an alpha helical motif sufficient for association with papillomavirus E6. J. Biol. Chem. 1998; 273:13537–13544. [PubMed: 9593689]

Cooper B, Schneider S, Bohl J, Jiang Y, Beaudet A, Vande Pol S. Requirement of E6AP and the features of human papillomavirus E6 necessary to support degradation of p53. Virology. 2003; 306:87–99. [PubMed: 12620801]

Cornilescu G, Delaglio F, Bax A. Protein backbone angle restraints from searching a database for chemical shift and sequence homology. J. Biomol. NMR. 1999; 13:289–302. [PubMed: 10212987]

de Souza RF, Iyer LM, Aravind L. Diversity and evolution of chromatin proteins encoded by DNA viruses. Biochim. Biophys. Acta. 2010; 1799:302–318. [PubMed: 19878744]

de Villiers EM, Fauquet C, Broker TR, Bernard HU, zur Hausen H. Classification of papillomaviruses. Virology. 2004; 324:17–27. [PubMed: 15183049]

de Vries SJ, van Dijk M, Bonvin AM. The HADDOCK web server for data-driven biomolecular docking. Nat. Protocols. 2010; 5:883–897.

DeLano, WL. The PyMOL Molecular Graphics System DeLano Scientific. San Carlos, CA:

Dominguez C, Boelens R, Bonvin AM. HADDOCK: a protein-protein docking approach based on biochemical or biophysical information. J. Am. Chem. Soc. 2003; 125:1731–1737. [PubMed: 12580598]

Farrow NA, Muhandiram R, Singer AU, Pascal SM, Kay CM, Gish G, Shoelson SE, Pawson T, Forman-Kay JD, Kay LE. Backbone dynamics of a free and phosphopeptide-complexed Src homology 2 domain studied by 15N NMR relaxation. Biochemistry. 1994; 33:5984–6003. [PubMed: 7514039]

Garcia-Alai MM, Dantur KI, Smal C, Pietrasanta L, de Prat-Gay G. High-risk HPV E6 oncoproteins assemble into large oligomers that allow localization of endogenous species in prototypic HPV-transformed cell lines. Biochemistry. 2007; 46:341–349. [PubMed: 17209544]

Giovane C, Trave G, Briones A, Lutz Y, Wasylyk B, Weiss E. Targetting of the N-terminal domain of the human papillomavirus type 16 E6 oncoprotein with monomeric ScFvs blockes the E6-mediated degradation of cellular p53. J. Mol. Recognition. 1999; 12:141–152.

Glaunsinger B, Lee S, Thomas M, Banks L, Javier R. Interactions of the PDZ-protein MAGI-1 with adenovirus E4-ORF1 and high-risk papillomavirus E6 oncoproteins. Oncogene. 2000; 19:5270–5280. [PubMed: 11077444]

Grishin NV. Treble clef finger--a functionally diverse zinc-binding structural motif. Nucleic Acids Res. 2001; 29:1703–1714. [PubMed: 11292843]

Gross-Mesilaty S, Reinstein E, Bercovich B, Tobias K, Schwartz A, Kahana C, Ciechanover A. Basal and human papillomavirus E6 oncoprotein-induced degradation of Myc proteins by the ubiquitin pathway. Proc. Natl. Acad. Sci. U S A. 1998; 95:8058–8063. [PubMed: 9653139]

Gu J, Rubin R, Yuan Z. A sequence element of p53 that determines its susceptibility to viral oncoprotein-targeted degradation. Oncogene. 2001; 20:3519–3527. [PubMed: 11429698]

Herrmann T, Guntert P, Wuthrich K. Protein NMR structure determination with automated NOE assignment using the new software CANDID and the torsion angle dynamics algorithm DYANA. J. Mol. Biol. 2002a; 319:209–227. [PubMed: 12051947]

Herrmann T, Guntert P, Wuthrich K. Protein NMR structure determination with automated NOE-identification in the NOESY spectra using the new software ATNOS. J. Biomol. NMR. 2002b; 24:171–189. [PubMed: 12522306]

Huibregtse JM, Scheffner M, Howley PM. A cellular protein mediates association of p53 with the E6 oncoprotein of human papillomavirus types 16 or 18. EMBO J. 1991; 10:4129–4135. [PubMed: 1661671]

Huibregtse JM, Scheffner M, Howley PM. Localization of the E6-AP regions that direct human papillomavirus E6 binding, association with p53, and ubiquitination of associated proteins. Mol. Cell. Biol. 1993; 13:4918–4927. [PubMed: 8393140]

Jing M, Bohl J, Brimer N, Kinter M, Vande Pol SB. Degradation of tyrosine phosphatase PTPN3 (PTPH1) by association with oncogenic human papillomavirus E6 proteins. J. Virol. 2007; 81:2231–2239. [PubMed: 17166906]

Kao WH, Beaudenon SL, Talis AL, Huibregtse JM, Howley PM. Human papillomavirus type 16 E6 induces self-ubiquitination of the E6AP ubiquitin-protein ligase. J. Virol. 2000; 74:6408–6417. [PubMed: 10864652]

Kiyono T, Hiraiwa A, Fujita M, Hayashi Y, Akiyama T, Ishibashi M. Binding of high-risk human papillomavirus E6 oncoproteins to the human homologue of the Drosophila discs large tumor suppressor protein. Proc. Natl. Acad. Sci. U S A. 1997; 94:11612–11616. [PubMed: 9326658]

Koradi R, Billeter M, Wuthrich K. MOLMOL: a program for display and analysis of macromolecular structures. J. Mol. Graph. 1996; 14:51–55. 29–32. [PubMed: 8744573]

Laskowski RA, Rullmannn JA, MacArthur MW, Kaptein R, Thornton JM. AQUA and PROCHECK-NMR: programs for checking the quality of protein structures solved by NMR. J. Biomol. NMR. 1996; 8:477–486. [PubMed: 9008363]

Li X, Coffino P. High-risk Human Papillomavirus E6 protein has two distinct binding sites within p53, of which one determines degradation. J. Virol. 1996; 70:4509–4516. [PubMed: 8676476]

Linge JP, Williams MA, Spronk CA, Bonvin AM, Nilges M. Refinement of protein structures in explicit solvent. Proteins. 2003; 50:496–506. [PubMed: 12557191]

Lipari F, McGibbon GA, Wardrop E, Cordingley MG. Purification and biophysical characterization of a minimal functional domain and of an N-terminal Zn^{2+}-binding fragment from the human papillomavirus type 16 E6 protein. Biochemistry. 2001; 40:1196–1204. [PubMed: 11170444]

Liu Y, Chen JJ, Gao Q, Dalal S, Hong Y, Mansur CP, Band V, Androphy EJ. Multiple functions of human papillomavirus type 16 E6 contribute to the immortalization of mammary epithelial cells. J. Virol. 1999; 73:7297–7307. [PubMed: 10438818]

Liu Y, Cherry JJ, Dineen JV, Androphy EJ, Baleja JD. Determinants of stability for the E6 protein of papillomavirus type 16. J. Mol. Biol. 2009; 386:1123–1137. [PubMed: 19244625]

Massimi P, Shai A, Lambert P, Banks L. HPV E6 degradation of p53 and PDZ containing substrates in an E6AP null background. Oncogene. 2008; 27:1800–1804. [PubMed: 17934525]

Masson M, Hindelang C, Sibler A, Trave G, Weiss E. Preferential nuclear sublocalization of HPV16 E6 oncoprotein in cervical carcinoma cells. J. Gen. Virol. 2003; 84:2099–2104. [PubMed: 12867640]

Nabuurs SB, Nederveen AJ, Vranken W, Doreleijers JF, Bonvin AM, Vuister GW, Vriend G, Spronk CA. DRESS: a database of refined solution NMR structures. Proteins. 2004; 55:483–486. [PubMed: 15103611]

Nominé Y, Charbonnier S, Miguet L, Potier N, Van Dorsselaer A, Travé G, Kieffer B. ^{1}H and ^{15}N resonance assignment, secondary structure and dynamic behaviour of the C-terminal domain of human papillomavirus oncoprotein E6. J. Biomol. NMR. 2005

Nominé Y, Charbonnier S, Ristriani T, Stier G, Masson M, Cavusoglu N, Van Dorsselaer A, Weiss E, Kieffer B, Travé G. Domain substructure of HPV E6 protein: biophysical characterization of E6 C-terminal DNA-binding domain. Biochemistry. 2003; 42:4909–4917. [PubMed: 12718532]

Nomine Y, Masson M, Charbonnier S, Zanier K, Ristriani T, Deryckere F, Sibler AP, Desplancq D, Atkinson RA, Weiss E, et al. Structural and functional analysis of E6 oncoprotein: insights in the molecular pathways of human papillomavirus-mediated pathogenesis. Mol. Cell. 2006; 21:665–678. [PubMed: 16507364]

Nominé Y, Ristriani T, Laurent C, Lefèvre JF, Weiss E, Travé G. A strategy for optimizing the monodispersity of fusion proteins: application to purification of recombinant HPV E6 oncoprotein. Protein Eng. 2001a; 14:297–305.

Nominé Y, Ristriani T, Laurent C, Lefèvre JF, Weiss E, Travé G. Formation of soluble inclusion bodies by HPV E6 oncoprotein fused to Maltose-binding protein. Protein Expr. Purif. 2001b; 23:22–32.

Ould M'hamed Ould Sidi A, Ould Babah K, Brimer N, Nomine Y, Romier C, Kieffer B, Vande Pol S, Trave G, Zanier K. Strategies for bacterial expression of protein-peptide complexes: application to solubilization of papillomavirus E6. Protein Expr. Purif. 2011; 80:8–16. [PubMed: 21777678]

Ristriani T, Fournane S, Orfanoudakis G, Trave G, Masson M. A single-codon mutation converts HPV16 E6 oncoprotein into a potential tumor suppressor, which induces p53-dependent senescence of HPV-positive HeLa cervical cancer cells. Oncogene. 2009; 28:762–772. [PubMed: 19015633]

Sattler M, Schleucher M, Griesinger C. Heteronuclear multidimensional NMR experiments for the structure determination of proteins in solution employing pulsed field gradients. Prog. NMR Spectrosc. 1999; 34:93–158.

Scheffner M, Huibregtse JM, Vierstra RD, Howley PM. The HPV-16 E6 and E6-AP complex functions as a ubiquitin-protein ligase in the ubiquitination of p53. Cell. 1993; 75:495–505. [PubMed: 8221889]

Scheffner M, Nuber U, Huibregtse J. Protein ubiquitination involving an E1-E2-E3 enzyme ubiquitin thioester cascade. Nature. 1995; 373:81–83. [PubMed: 7800044]

Schuck P. Size-distribution analysis of macromolecules by sedimentation velocity ultracentrifugation and lamm equation modeling. Biophys. J. 2000; 78:1606–1619. [PubMed: 10692345]

Schwieters CD, Kuszewski JJ, Tjandra N, Clore GM. The Xplor-NIH NMR molecular structure determination package. J. Magn. Reson. 2003; 160:65–73. [PubMed: 12565051]

Shai A, Nguyen ML, Wagstaff J, Jiang YH, Lambert PF. HPV16 E6 confers p53-dependent and p53-independent phenotypes in the epidermis of mice deficient for E6AP. Oncogene. 2007; 26:3321–3328. [PubMed: 17130828]

Stewart D, Kazemi S, Li S, Massimi P, Banks L, Koromilas A, Matlashewski G. Ubiquitination and proteasome degradation of the E6 proteins of human papillomavirus types 11 and 18. J. Gen. Virol. 2004; 85:1419–1426. [PubMed: 15166424]

Thomas M, Banks L. Inhibition of Bak-induced apoptosis by HPV-18 E6. Oncogene. 1998; 17:2943–2954. [PubMed: 9881696]

Thomas M, Chiang C. E6 oncoprotein represses p53-dependent gene activation via inhibition of protein acetylation independently of inducing p53 degradation. Mol. Cell. 2005; 17:251–264. [PubMed: 15664194]

Thomas M, Laura R, Hepner K, Guccione E, Sawyers C, Lasky L, Banks L. Oncogenic human papillomavirus E6 proteins target the MAGI-2 and MAGI-3 proteins for degradation. Oncogene. 2002; 21:5088–5096. [PubMed: 12140759]

Tomaic V, Pim D, Banks L. The stability of the human papillomavirus E6 oncoprotein is E6AP dependent. Virology. 2009; 393:7–10. [PubMed: 19700180]

Tomaic V, Pim D, Thomas M, Massimi P, Myers MP, Banks L. Regulation of the human papillomavirus type 18 E6/E6AP ubiquitin ligase complex by the HECT domain-containing protein EDD. J. Virol. 2011; 85:3120–3127. [PubMed: 21228227]

Topffer S, Muller-Schiffmann A, Matentzoglu K, Scheffner M, Steger G. Protein tyrosine phosphatase H1 is a target of the E6 oncoprotein of high-risk genital human papillomaviruses. J. Gen. Virol. 2007; 88:2956–2965. [PubMed: 17947517]

Vos RM, Altreuter J, White EA, Howley PM. The ubiquitin-specific peptidase USP15 regulates human papillomavirus type 16 E6 protein stability. J. Virol. 2009; 83:8885–8892. [PubMed: 19553310]

Werness BA, Levine AJ, Howley PM. Association of human papillomavirus types 16 and 18 E6 proteins with p53. Science. 1990; 248:76–79. [PubMed: 2157286]

Zanier K, Charbonnier S, Baltzinger M, Nomine Y, Altschuh D, Trave G. Kinetic analysis of the interactions of Human Papillomavirus E6 oncoproteins with the ubiquitin ligase E6AP using Surface Plasmon Resonance. J. Mol. Biol. 2005; 349:401–412. [PubMed: 15890204]

Zanier K, Nomine Y, Charbonnier S, Ruhlmann C, Schultz P, Schweizer J, Trave G. Formation of well-defined soluble aggregates upon fusion to MBP is a generic property of E6 proteins from various human papillomavirus species. Protein Expr. Purif. 2007; 51:59–70. [PubMed: 17055740]

Zanier K, Ruhlmann C, Melin F, Masson M, Ould M'hamed Ould Sidi A, Bernard X, Fischer B, Brino L, Ristriani T, Rybin V, et al. E6 proteins from diverse papillomaviruses self-associate both in vitro and in vivo. J. Mol. Biol. 2010; 396:90–104. [PubMed: 19917295]

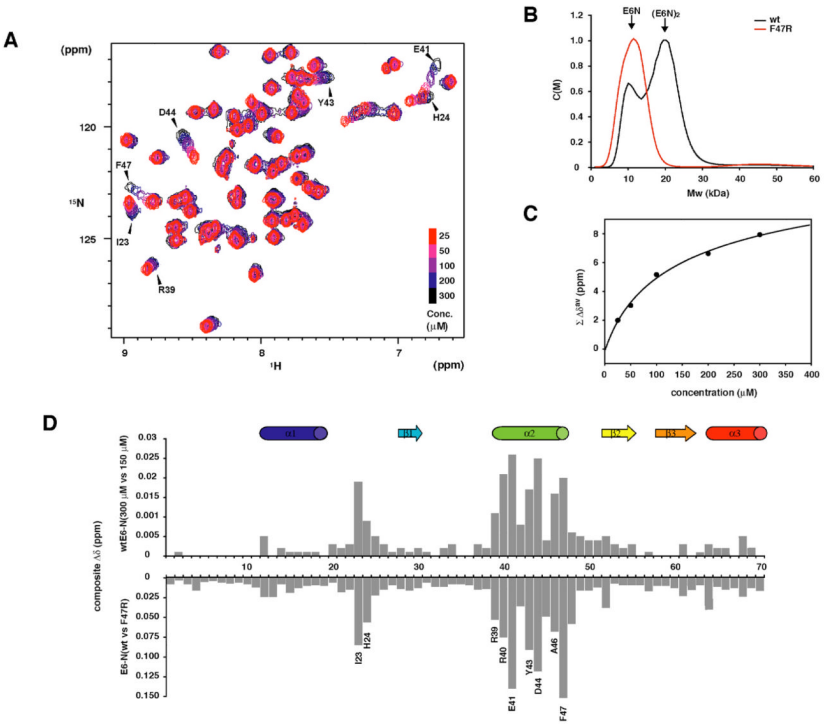

Figure 1.

Dimerization of the HPV16 E6N domain. **(A)** Superimposition of a region of the ^{1}H-^{15}N HSQC spectra of the wild-type HPV16 E6N domain measured at concentrations of 25 (red), 50 (magenta), 100 (violet), 200 (blue) and 300 (black) μM. Amide groups undergoing significant shifts are labelled. (**B**) Molecular weight distribution of wild-type and F47R HPV16 E6N constructs derived from sedimentation velocity ultracentrifugation experiments. The molecular weights of E6N monomeric (E6N) and dimeric ($(E6N)_2$) species are indicated. C(M) indicates arbitrary units. (**C)** Estimation of the equilibrium affinity constant (K_D) of wild-type HPV16 E6N dimerization. The sum of the chemical shift changes from four selected amide cross-peaks (belonging to residues H24, E41, D44, F47) are plotted against the total concentration of the E6N domain. $\Delta\delta = (10*(\delta H-\delta H_0)^2 + ((\delta N-\delta N_0)^2)^{1/2}$ where δH and δN are the proton and nitrogen chemical shifts of each residue, while δH_0 and δN_0 are the proton and nitrogen chemical shifts at 25 μM. The K_D value derived from the fit corresponds to 290 ± 120 μM. (**D**) Chemical shift perturbations induced by dilution of the wt E6N sample (wt E6N at 300 μM versus 150 μM) (*upper plot*) and introduction of the F47R mutation (corresponding to chemical shift differences between wtE6N at 300 μM versus E6N F47R) (*lower plot*). The y-axis of the lower plot has been inverted for clarity. Δδ is a composite shift obtained by combining on a per-residue basis the chemical shift changes for all assigned ^{1}H, ^{13}C and ^{15}N. Composite $\Delta\delta=\frac{1}{N}\left(\sum_{i=1}^{N}\frac{\Delta\nu_i^2}{\sigma_i}\right)^2$ where *N* is the number of nuclei, Δν is the chemical shift displacement and σ is the spectral dispersity factor of each nucleus derived from the BMRB data bank. Residues undergoing chemical shift displacements ≥ 0.0075 ppm upon wt E6N dilution or ≥0.050 ppm upon introduction of the F47R mutation are indicated. Secondary structure elements are derived from the 3D structure of the E6N F47R domain (see Figure 2). The colour coding of secondary structure elements will be retained in subsequent figures. See also Figure S1.

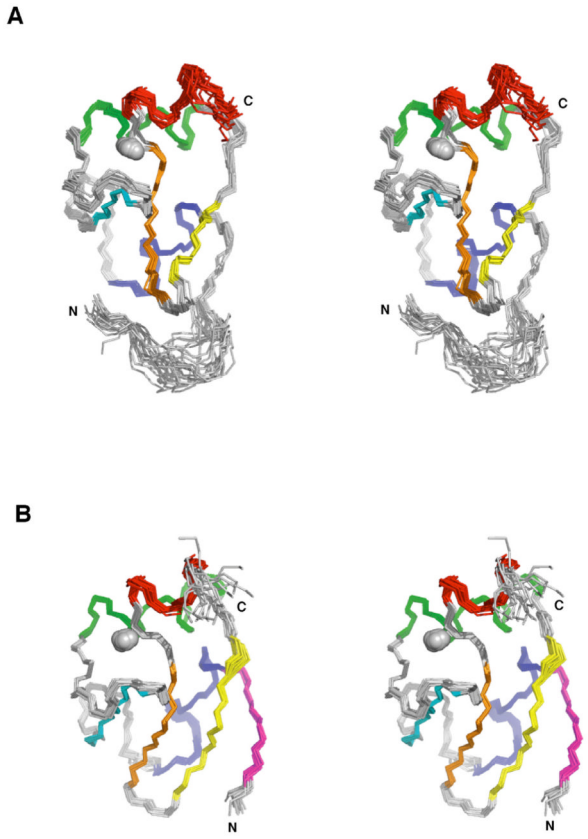

Figure 2.
NMR ensembles of the E6 domain structures. Stereo views of the 20 lowest energy structures of E6N F47R (residues 1-71) (**A**) and E6C 4C/4S (residues 80-143) (**B**). Zinc atoms are represented as grey spheres. Figures of the molecular structures were made using PyMOL (DeLano). See also Figure S2.

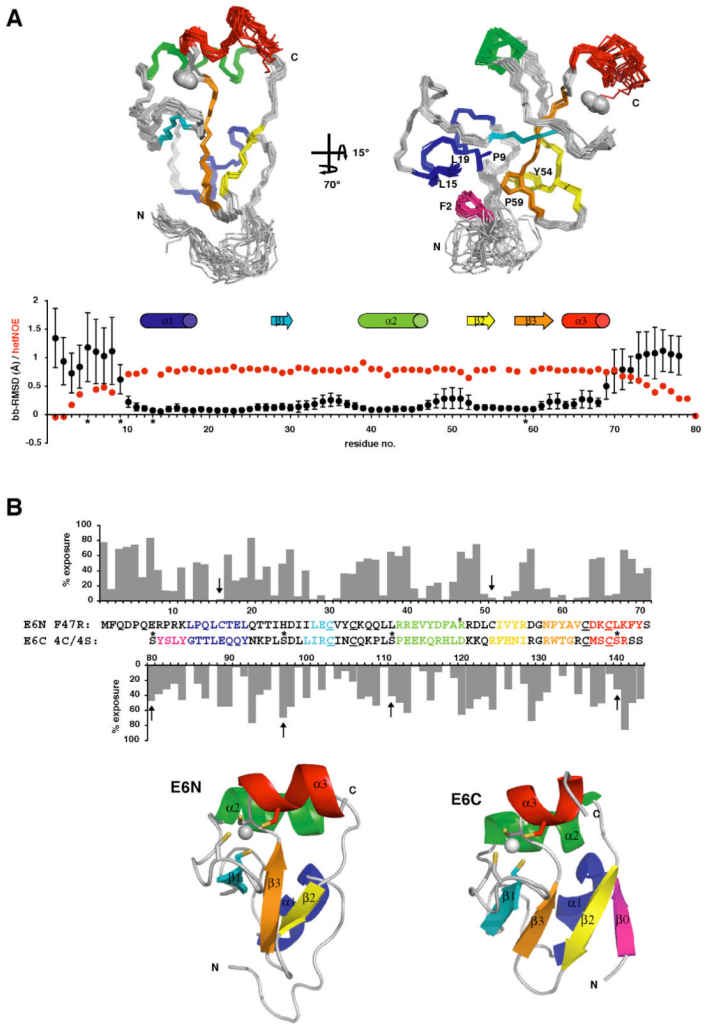

Figure 3.

Structure and dynamic properties of the monomeric HPV16 E6 zinc-binding domains. (**A**) (*Upper panel*) Ensemble of the 20 lowest energy structures of E6N F47R. The right hand view shows the anchoring residue F2 and other hydrophobic core residues displaying NOE contacts with F2. (*Lower panel*) Heteronuclear NOE (red circles) and average pairwise backbone r.m.s. deviations (black circles) values for the E6N F47R domain. R.m.s. deviations have been calculated over five residue segments of the primary sequence for the 20 lowest energy NMR structures and error bars represent standard deviations of the mean. Black stars on the x-axis mark proline residues. (**B**) Structural homology of the E6N and E6C domains (*Upper panel*) Percentage of exposure to the solvent of residues in the lowest energy NMR structures of E6N F47R and E6C-4C/4S constructs. The y-axis of the E6C plot has been inverted for clarity. Numbers on the x-axis correspond to the wild-type HPV16 E6 sequence. The amino acid sequence of each domain is aligned with the x-axis and coloured to mark secondary structure elements. Zinc coordinating cysteines are underligned, while exposure values for non-conserved cysteines are indicated by arrows. Asterisks indicate sites of mutations. (*Lower panel*) Ribbon representations of the lowest energy NMR structures of the E6N F47R (left) and E6C 4C/4S (right) constructs. Zinc atoms and coordinating cysteine side-chains are displayed. See also Figure S3.

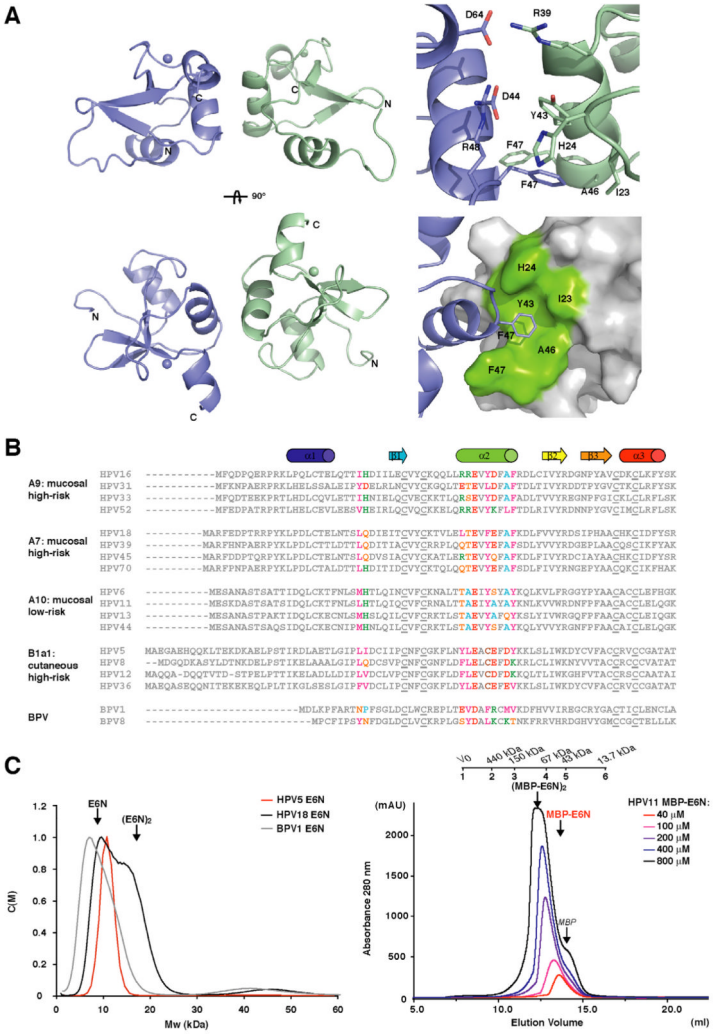

Figure 4.

Model structure of the HPV16 E6N homodimer. (**A**) (*Left panel*) Ribbon representation of the lowest energy structure in cluster 1. (*Right panel*) Views of the homodimer interface. The top representation illustrates the side-chain orientation of interacting residues. The bottom representation illustrates the positioning of the aromatic ring F47 (violet) in the shallow hydrophobic pocket (green) within the opposing subunit. (**B**) Alignment of E6N sequences of representative strains from the “high-risk” mucosal HPV A9 and A7 groups, the low-risk mucosal A10 group, the “high-risk” cutaneous B1A1 group and two BPV strains. Residues reported to undergo the largest chemical shift variations in Figure 1D are coloured according to their physicochemical properties as follows: magenta, hydrophobic (W, F, Y, L, I, V, M); green, basic (K, R, H); red, acidic (E, D); orange, polar (Q, N, T, S); brown, cystein (C); cyan, small (G, A, P). (**C**) (*Left panel*) Molecular weight distribution of wild-type HPV5, HPV18 and BPV1 E6N domain constructs derived from sedimentation velocity ultracentrifugation experiments. (*Right panel*) Analytical gel filtration chromatography analysis of affinity purified HPV11 MBP-E6N fusion construct. Samples were adjusted at the concentrations indicated and injected on a Superdex 200 10/30 column. The elution volumes of the monomeric (MBP-E6N, 55.2 kDa) and dimeric ($(MBP\text{-}E6N)_2$, 110.4 kDa) species are indicated. The shoulder at 14.1 ml corresponds to MBP arising from residual proteolytic activity in the preparations. Molecular size markers are reported on top

of the figure. “1,” V_0; “2,” ferritin (440 kDa); “3,” mouse immunoglobulin G (150 kDa); “4,” bovine serum albumin (67 kDa); “5,” ovoalbumin (43 kDa); “6,” RNase (13.7 kDa). See also Figure S4.

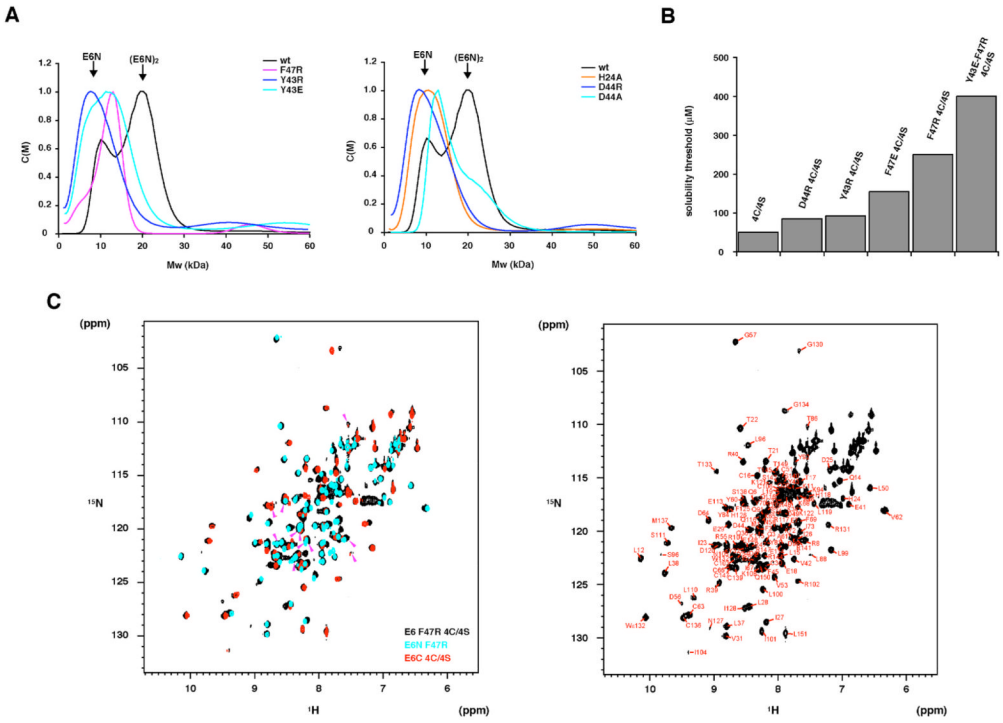

Figure 5.

Mutations at the E6N homodimer interface enhance full-length E6 solubility. (**A**) Homodimer interface mutations have been introduced in the context of HPV16 E6N domain construct and the resulting samples have been analyzed by sedimentation velocity ultracentrifugation experiments. The profile of the wild-type domain is reported on each plot for clarity. (**B**) Concentrations thresholds of samples of full-length E6 mutants. Homodimer interface mutations have been introduced in the HPV16 E6 4C/4S construct. (**C**) ^{1}H, ^{15}N HSQC spectra of the E6 F47R 4C/4S construct. (*Left panel*) Superposition of spectra of E6 F47R 4C/4S (black), E6N F47R (cyan) and E6C 4C/4S (red) constructs. Magenta arrows indicate amide groups belonging to residues 1-10 and 80-90. (*Right panel)* Annotated ^{1}H, ^{15}N HSQC of E6 F47R 4C/4S. Assignments are shown in red. See also Figure S5.

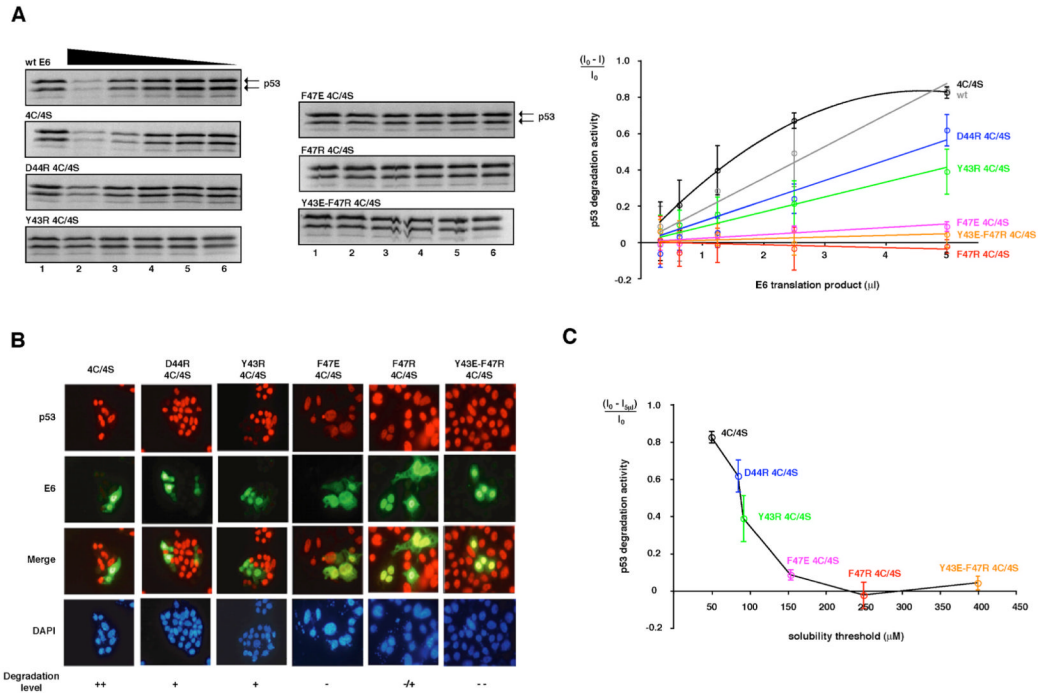

Figure 6.

p53 degradation activities of HPV16 E6 homodimer interface mutants. (**A**) *In vitro* p53 degradation reactions employing *in vitro* translated and ^{35}S labelled proteins. Assays were performed by incubating 2 µl of ^{35}S p53 translation product with varying amounts of ^{35}S E6 translation products. In the input control the reaction was stopped immediately after mixing p53 and E6 by addition of loading buffer. (*Left panel*) Partial views of the autoradiographs showing the p53 double band after incubation with different amounts of the E6 mutants. For clarity, the E6 bands for each of the p53 degradation reactions are shown separately in Figure S6B. Lane 1 (L1): input; L2: 5 µl E6; L3: 2.5 µl E6; L4: 1.25 µl E6; L5: 0.75 µl E6; L6: 0.37 µl E6. (*Right panel*) Plot summarizing the *in vitro* p53 degradation profiles of the different E6 mutants. The p53 degradation activity is represented as $(I_0\text{-}I)/I_0$ where I is the intensity of the p53 double band after incubation with E6 while I_0 p53 signal in the input lane. Error bars represent standard deviations from three independent experiments. **(B)** Double immunofluorescence of E6 and p53 in C33A cells after transfection with wt E6 or E6 mutants. Observation of p53 and E6 was achieved by incubating cells first with the anti-p53 antibody and then with the anti-E6 antibody. The disappearance of the red p53 signal in E6 transfected cells displaying a green signal indicates E6 mediated p53 degradation. (**C**) Correlation of p53 degradation activities and solubility thresholds of the different E6 mutants. The $(I_0\text{-}I_{5\mu l})/I_0$ ratio refers to the *in vitro* p53 degradation in the presence of 5 µl of E6. See also Figure S6.

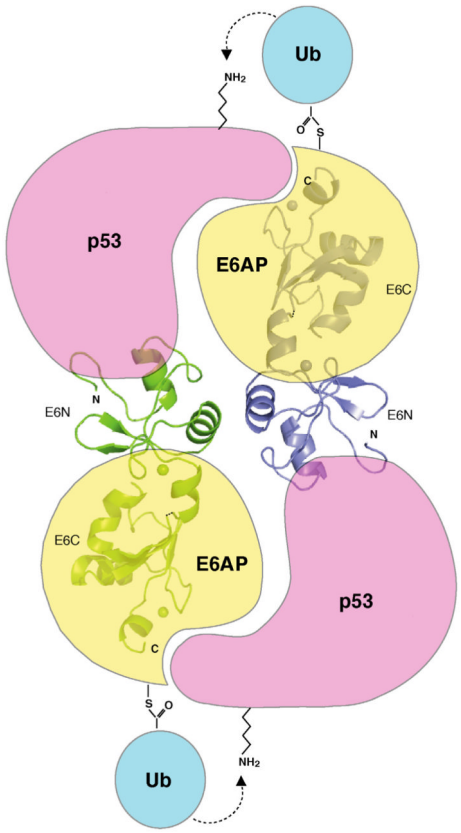

Figure 7.

Putative model of the E6/E6AP/p53 trimery complex. At the center the ribbon representation of a symmetric dimer of E6 mediated by the E6N domains. The two subunits of the dimer are shown in green and violet respectively. The relative orientation of the E6N and E6C domains is arbitrary. Each E6 molecule binds to one molecule of E6AP (yellow cartoon) and one molecule of p53 (pink cartoon). In this model, only ubiquitin transfer events are possible that originate between E6AP and p53 molecules loaded on different subunits of the E6 dimer.

Table 1
NMR and refinement statistics for the E6N and E6C domain structures

	E6N	E6C
Restraints for final calculation		
Total NOE	1274	1464
Intra-residue	433	370
Inter-residue		
Sequential (|i − j| = 1)	311	366
Medium-range (|i − j| < 5)	240	357
Long-range (|i − j| > 5)	290	371
Hydrogen bonds	7	2
Total dihedral angle restraints (φ, ψ)	87	92
Structure statistics		
R.m.s. deviations from idealised geometry		
Bonds (Å)	0.017 ±0.001	0.017 ±0.001
Bond angles (°)	1.880 ±0.050	2.160 ±0.050
Impropers (°)	1.790 ±0.080	1.980 ±0.080
NOE restraints (Å)	0.045 ±0.001	0.043 ±0.001
Dihedral angle restraints (°)	0.510±0.130	0.490 ±0.050
Violations[a]		
Max. dihedral angle violation (°)	4.80	3.54
Max. NOE violation (Å)	0.39	0.47
Ramachandran plot[b]		
Residues in most favourable regions (%)	80.5	78.0
Residues in additional favourable regions (%)	16.8	21.0
Residues in generously favourable regions (%)	0.5	0.7
Residues in disallowed regions (%)	2.2	0.4
Coordinate precision[b]		
Average pairwise r.m.s. deviation (Å)[c]		
Heavy	1.48 ± 0.19	1.13 ± 0.15
Backbone	0.82 ± 0.14	0.56 ± 0.14

Statistics are given for the 20 lowest-energy structures after water refinement out of 100.

[a] No distance restraint was violated by > 0.5 Å and no dihedral angle restraint by > 5°.

[b] Calculated for residues 12 to 72 (E6N) and residues 80 to 143 (E6C).

[c] Pairwise r.m.s. deviations were calculated using MOLMOL (Koradi et al., 1996)).

Table 2
Statistics of the best E6N homodimer models

NMR restraints[a]	
Ambigous restraints (AIRs)	16
Intermaolecular NOE-derived unambigous restraints	22
Total dihedral angle restraints (φ, ψ)	74
Structure statistics	
R.m.s. deviations from idealised geometry[b]	
AIRs (Å)	0.14±0.11
NOE restraints (Å)	0.00±0.01
Dihedral angle restraints (°)	0.54±0.12
Coordinate precision[c]	
Average pairwise r.m.s. deviation (Å)	
Backbone	2.2±0.8
Intermolecular energies after water refinement	
E_{vdw}(kcal mol^{-1})	−35±5
E_{elec}(kcal mol^{-1})	119±43
Buried surface area (Å)	975±90

Statistics for the 20 best-scoring models in cluster1.

[a] Restraints have been applied symmetrically to each homodimer subunit.

[b] No distance restraint was violated by > 0.1 Å and no dihedral angle restraint by > 5°.

[c] Pairwise r.m.s. deviations calculated for residues 12 to 72.